INDUCTIVE MEGAHERTZ BEAM POSITION MONITORS FOR CEBAF

Walter Barry
Continuous Electron Beam Accelerator Facility
12000 Jefferson Avenue, Newport News, VA 23606

Abstract

CEBAF is a CW five pass recirculating linac with an energy gain of 800 MeV per pass. As a result, multiple beams of different energies are present simultaneously in the straight section beamlines. In these sections, it is required that the position of each beam be measured separately. One method of accomplishing this involves modulating the beam current for a duration of less than one revolution period. With a modulated beam, position can be measured by either a multi-gigahertz pickup operating at a harmonic of the 1.5 GHz RF, or a pickup that responds to the lower modulation frequency. In this paper, the concepts of a simple inductive loop beam position monitor system based on the detection of a 1-10 MHz amplitude modulated beam are presented.

Introduction

In the linac sections of the CEBAF accelerator, up to five beams of different energies may be present simultaneously in the same vacuum chamber. In order to track the transverse position of a single beam during each of its passes, a method of distinguishing it from the other beams is necessary. One method of accomplishing this is to sinusoidally amplitude modulate the CW beam for a duration of less than the circulation time in the machine (4.2 μsec). In addition, the time interval between modulation bursts should be greater than five circulations (21 μsec) so as to allow a given burst to exit the machine before the next one is introduced. During normal operation of the accelerator, the modulation is impressed on the beam from time to time without interrupting the continuous flow of electrons. A beam position monitor that responds to the modulation frequency provides the capability to measure the position of a single beam from entrance to exit. In order to make the same measurement with RF monitors, the continuous flow of the beam has to be interrupted. However, during the time the beam is not modulated, the current design plan calls for 3 GHz sum and difference mode cavity pairs for continuous beam position monitoring.[1]

The low frequency monitors to be described in this paper consist of simple inductive loops inside the vacuum chamber. For several practical reasons to be discussed, the operating frequency of the monitors is in the 1–10 MHz range. Because of the simple loop design and relative ease of designing electronics in the 1–10 MHz range, these monitors are excellent low cost alternatives to stripline or cavity monitors which work at some harmonic of the RF. The high cost of cavity and stripline monitors is attributed to stringent mechanical tolerances and expensive microwave electronics. In view of these cost differentials, it is currently proposed that loop monitors be used for all beam position measurements in tune–up or diagnostic modes of machine operation.

The majority of this paper is devoted to the theory of the inductive loop pickup. The equations relating difference to sum voltages to transverse beam position are derived first. Following this, the longitudinal and transverse pickup impedances for the loop monitor are calculated. Approximate relationships between difference to sum voltages and beam position along with a calibration scheme are then discussed. Finally, external electronics and initial test results are touched upon.

Inductive Loop Theory

A schematic side view and cross section of an inductive loop beam position monitor appears in Figure 1. The simple monitor consists of four rectangular loop pickups located inside the beampipe on the $\pm x$ and $\pm y$ axes as shown in Figure 1b. The terminal voltages at each pickup will be proportional to the time rate of change of the total magnetic flux intercepted by the loops in accordance with Faraday's law. The analysis of the loop monitor therefore consists of finding the voltages at all four terminals as a function of beam position r_0, ϕ_o. Several features of this particular problem simplify the analysis appreciably. For highly relativistic particles, the electric and magnetic fields are confined to the plane transverse to the beam. In addition, the beampipe and loop dimensions are extremely small compared to a wavelength in the 1–10 MHz range. As a result, the beam current may be considered to be uniform in z over the length of a loop and static electric and magnetic vector potentials may be used to determine the fields. However, AC boundary conditions are employed. Time harmonic fields and a perfectly conducting beampipe are assumed.

Referring to Figure 1, the voltage at the terminal of any loop is related to the beam

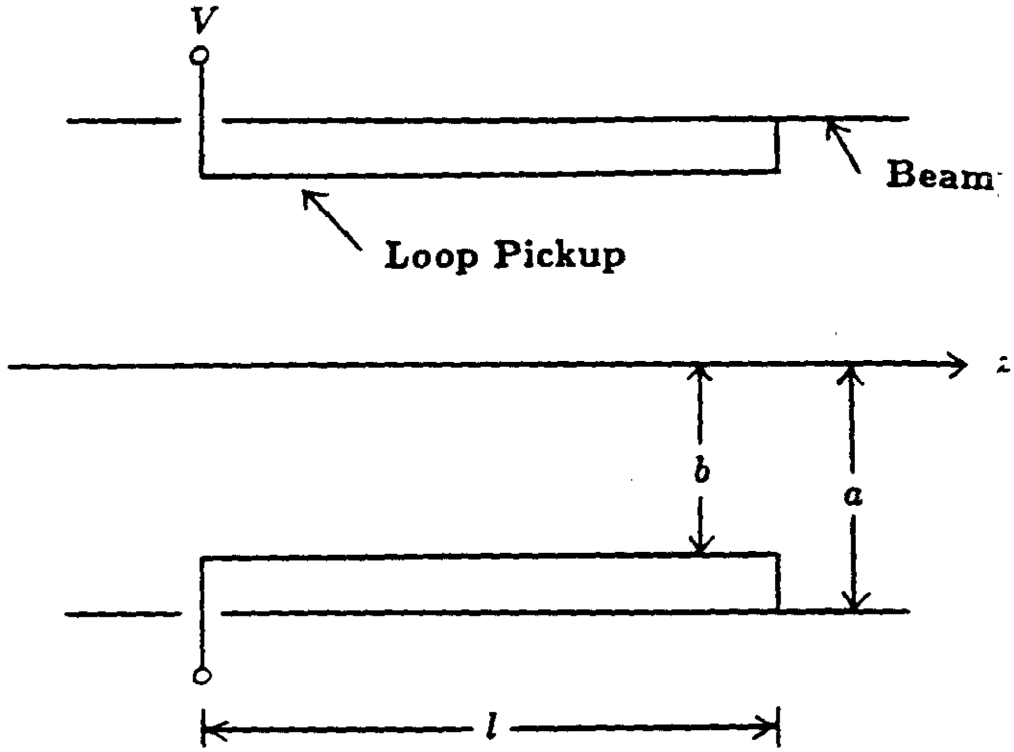

Figure 1a. Side view of inductive loop beam position monitor.

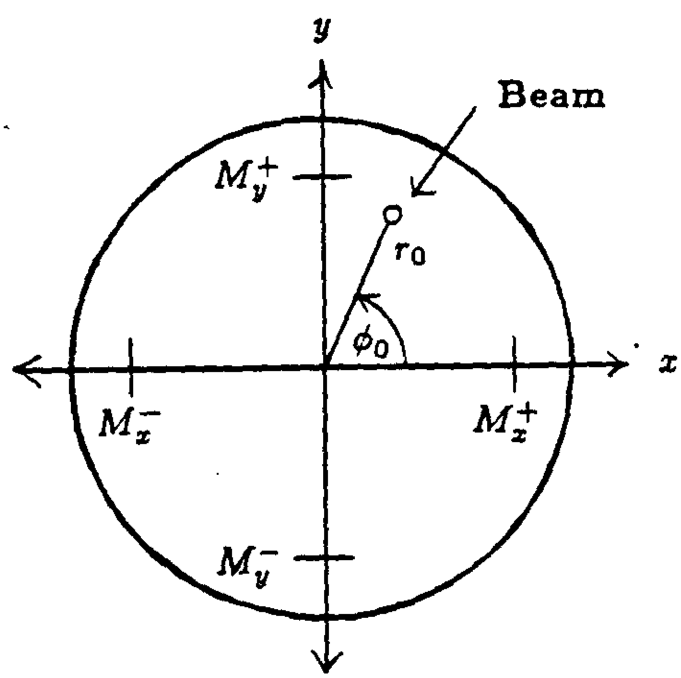

Figure 1b. Cross section of inductive loop beam position monitor.

current through the mutual inductance, M, between the beam and the loop:

$$V = j\omega M I_b \ . \tag{1}$$

The mutual inductance is a function of beam position relative to a given loop. Thus, for a given beam position, each loop has a mutual inductance designated in Figure 1b by M_x^+, M_x^-, M_y^+, and M_y^-. In order to obtain current independent position information, the standard technique of taking x and y difference to sum voltages is employed. Referring to Figure 1b and equation (1), the x and y difference to sum voltages, V_x and V_y, are defined by:

$$V_x = \frac{M_x^+ - M_x^-}{M_x^+ + M_x^-} \tag{2a}$$

$$V_y = \frac{M_y^+ - M_y^-}{M_y^+ + M_y^-} \ . \tag{2b}$$

From (2), it is seen that the difference to sum voltage responses are functions of the mutual inductances, which are in turn, dependent only on the geometry of the pickups.

The mutual inductance between the beam current and a loop is given by:

$$M = \frac{1}{I_b} \int_s \overrightarrow{B} \cdot \overrightarrow{ds} \ . \tag{3}$$

In (3), $\overrightarrow{B}$ is the magnetic flux from the beam and s is the surface enclosed by the loop. Atlernatively, using Stoke's theorem, M may be written as:

$$M = \frac{1}{I_b} \oint \overrightarrow{A} \cdot \overrightarrow{dl} \ , \tag{4}$$

where $\overrightarrow{A} = A_z$ is the vector potential for a beam current in the $\hat{z}$ direction. In (4), the path for the integral is the loop. Although it will not be needed, the $\overrightarrow{B}$ field can be calculated from $\overrightarrow{A}$ through:

$$\overrightarrow{B} = \nabla \times \overrightarrow{A} \ . \tag{5}$$

To calculate A_z, the method of images for uniform currents is employed. Boundary conditions require the $\overrightarrow{B}$ field to be zero inside the perfectly conducting beampipe wall. This implies a constant A_z everywhere on this boundary. As shown in Figure 2, this condition may be realized by removing the beampipe and placing an image current, $-I_b$, a distance r_i from the origin along the line adjoining the origin and I_b. The distance r_i is related to the beampipe radius, a, and the radial coordinate of the beam, r_0, by:[2]

$$r_i = a^2/r_0 \ . \tag{6}$$

The solution for A_z from I_b and its image will be valid everywhere inside the beampipe $(r \leq a)$.

In general, the vector potential may be derived from a volume integral over all source currents:

$$A_z(\overrightarrow{r}) = \frac{\mu_o}{4\pi} \int_{v'} \frac{J_z(\overrightarrow{r'})}{|\overrightarrow{r} - \overrightarrow{r'}|} dv' \ , \tag{7}$$

where:

$\overrightarrow{r'}$ = source position vector x', y', z'

$\overrightarrow{r}$ = field point position vector x, y, z

$|\overrightarrow{r} - \overrightarrow{r'}| = \sqrt{(x-x')^2 + (y-y')^2 + (z-z')^2}$.

In Figure 2, the beam current and its image are assumed to be line currents parallel to the z axis and infinite in extent. Therefore, the current density, J_z, in (7) may be written:

$$J_z(x', y') = I_b\delta(x' - x_0)\delta(y' - y_0) - I_b\delta(x' - x_i)\delta(y' - y_i) \ . \tag{8}$$

Because of symmetry, the integral in (7) may be computed for the $z = 0$ plane with no loss in generality. Substituting (8) into (7) and integrating over x' and y' while taking advantage of even symmetry about $z = 0$ yields:

$$A_z(x,y) = \frac{\mu_0 I_b}{2\pi} \int_0^\infty \left[\frac{1}{\sqrt{r_1^2 + z'^2}} - \frac{1}{\sqrt{r_2^2 + z'^2}} \right] dz' \; , \tag{9}$$

where:

$$r_1^2 = (x - x_0)^2 + (y - y_0)^2$$
$$r_2^2 = (x - x_i)^2 + (y - y_i)^2 \; .$$

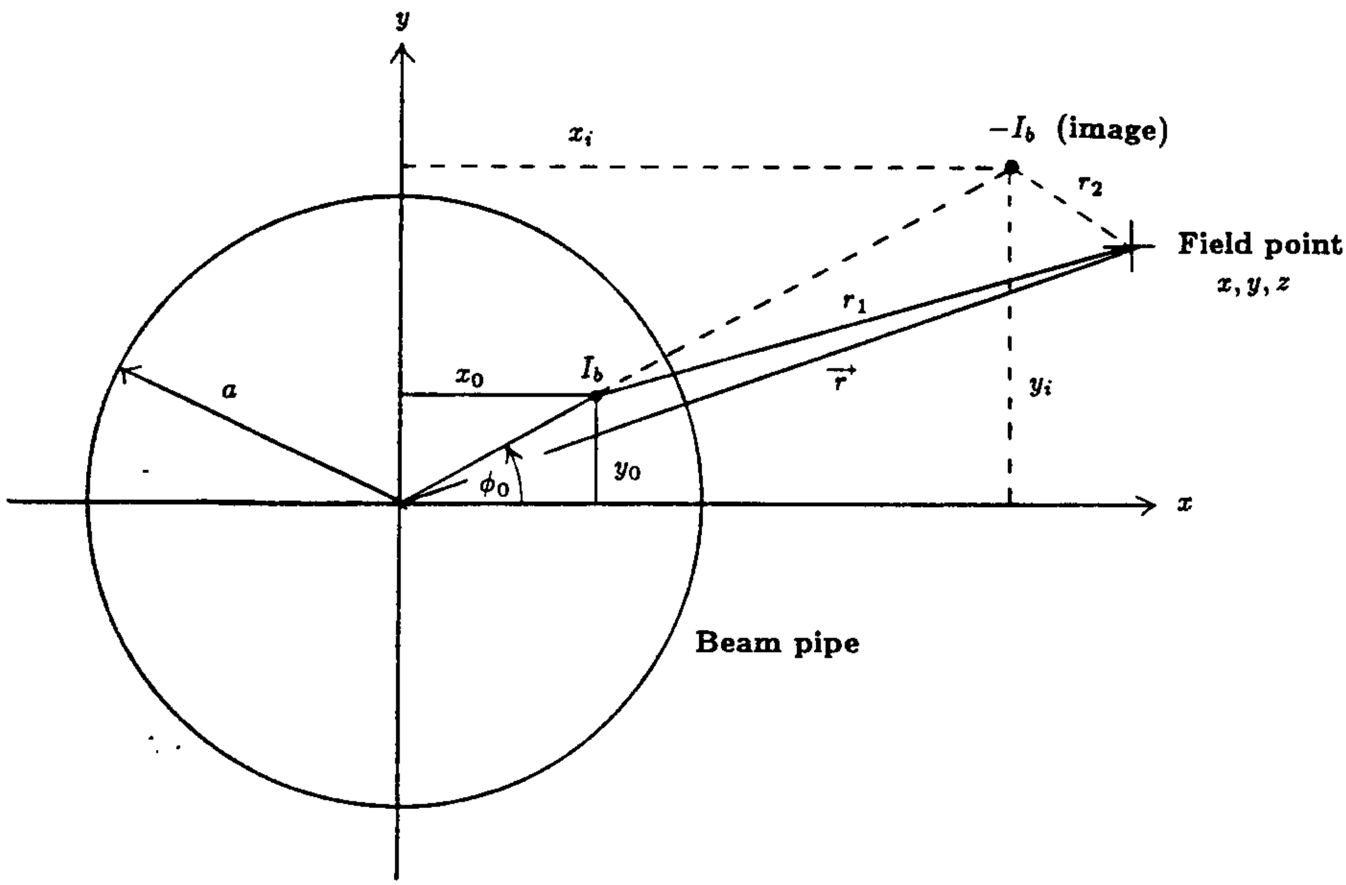

Figure 2 Geometry for calculating magnetic vector potential by method of images.

Performing the integral in (9) and converting to cylindrical coordinates gives the final expression for A_z:

$$A_z(r,\phi) = \frac{-\mu_0 I_b}{4\pi} \ln\left[\frac{r^2 + r_0^2 - 2rr_0\cos(\phi-\phi_0)}{r^2 + r_i^2 - 2rr_i\cos(\phi-\phi_0)}\right] , \tag{10}$$

where:

r_0, ϕ_0 are beam coordinates
$r_i = a^2/r_0$.

The mutual inductance between an axial beam current at position r_0, ϕ_0 and a rectangular loop pickup may be found from expression (4) where $\overrightarrow{A} = A_z$ is given by (10). The path for the integral is illustrated in Figure 3a. In Figure 3a, the loop is located at an arbitrary angle, ϕ, inside the beampipe and has a width $a - b$. The two short sections of the loop do not contribute to the integral in (4) because they are normal to the direction of $\overrightarrow{A}$. The mutual inductance between the beam current and the loop is then:

$$M = \frac{1}{I_b}\int_0^l A_z(b,\phi)dz + \int_l^0 A_z(a,\phi)dz . \tag{11}$$

Substituting (10) into (11) and performing the integrals yields the final expression for M:

$$M(r_o,\phi_0,\phi) = \frac{\mu_0 l}{4\pi}\ln\left[\frac{b^2r_0^2 - 2br_0\cos(\phi-\phi_0)+1}{r_0^2 - 2br_0\cos(\phi-\phi_0)+b^2}\right] . \tag{12}$$

In (12), a has been set equal to unity for convenience. Therefore, all radial coordinates and dimensions will be normalized to the beampipe radius a. The values of ϕ for the four pickups in Figure 1b are given in the following table:

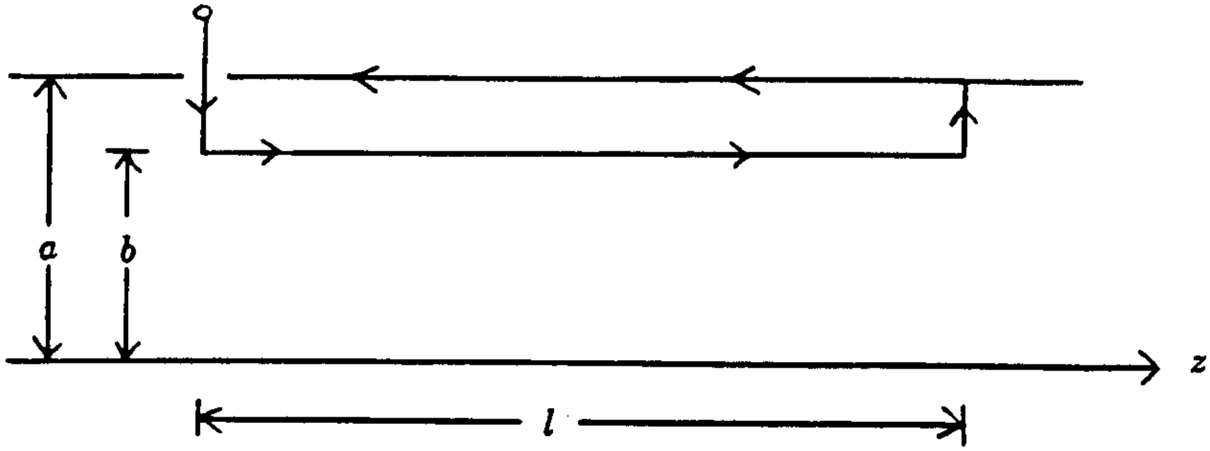

Figure 3a. Integration path for rectangular loop.

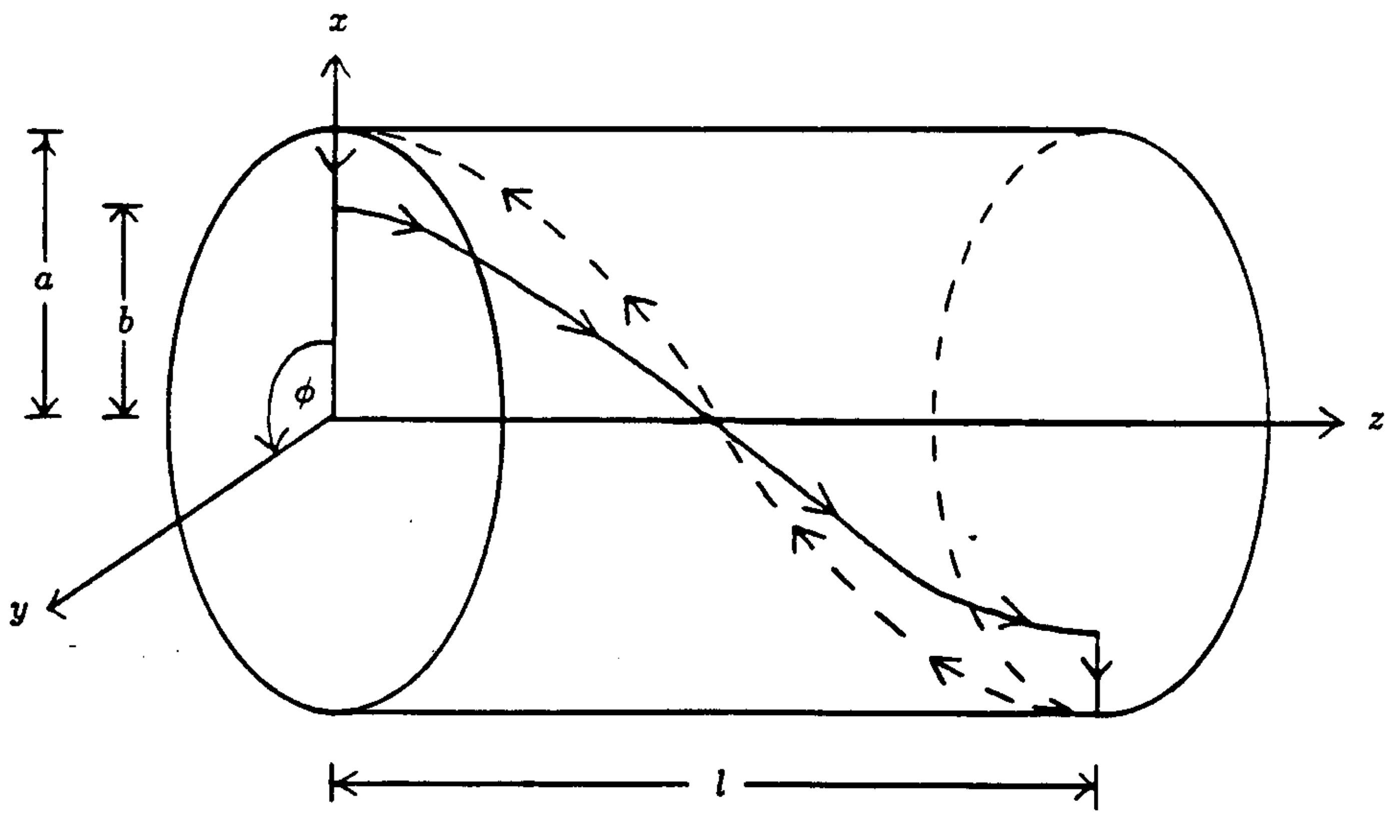

Figure 3b. Integration path for helical loop.

$\underline{M}$	$\underline{\phi}$
M_x^+	0
M_x^-	π
M_y^+	$\pi/2$
M_y^-	$3\pi/2$

Table 1. Rectangular loop pickup angles.

The x and y difference to sum voltages defined in (2) may now be evaluated as a function of beam position, r_0, ϕ_0, using the above values of ϕ and equation (12).

A plot of x difference to sum voltage, V_x, as a function of radial beam position for several azimuths from 0° to 90° is shown in Figure 4. Here, the normalized radial distance, b, to the pickups is taken to be .7. This translates to approximately .5" for the 1.4" I.D. beampipes in the CEBAF injector and linac sections. From Figure 4, the voltage response is seen to be a linear function of beam position for regions close to the origin.

In general, equations (2) and (12) constitute a mapping from the beam position plane to the difference to sum voltage plane, V_x, V_y. Further insight into the response of the loop monitor is obtained by mapping lines of constant x_0, y_0 into the V_x, V_y plane. This mapping for $b = .7$ is shown in Figure 5. In the V_x, V_y plane, the "squareness" of the grid sections indicates linearity and the curvature of the grid lines indicates the degree to which V_x depends on y_0 and V_y depends on x_0. Thus, a region with straight grid lines and square grid sections means V_x is a linear function of x_0 only and V_y is a linear function of y_0 only. As shown in Figure 5, this region is confined to the approximate area $r_0 < .2$. Outside this region, V_x and V_y are, in general, non-linear functions of both position coordinates.

In an attempt to expand the linear region of the monitor, the properties of helical loop pickups were investigated. In this case each loop follows a helical path subtending 180° in ϕ over the length of the monitor, l (Figure 3b). The mutual inductance is computed using equations (10) and (11) as with the planer loop, however the variable ϕ is now a function of z according to:

$$\phi = \frac{\pi z}{l} + \phi_s \ . \tag{13}$$

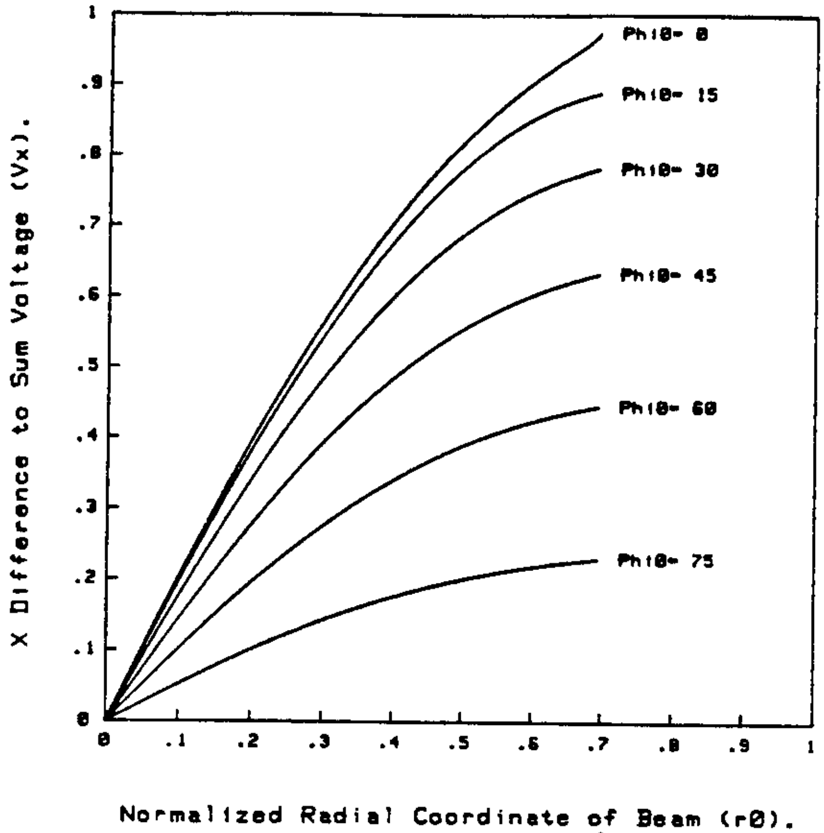

Figure 4. Planar loop monitor. V_x verses r_0 for several values of ϕ_0.

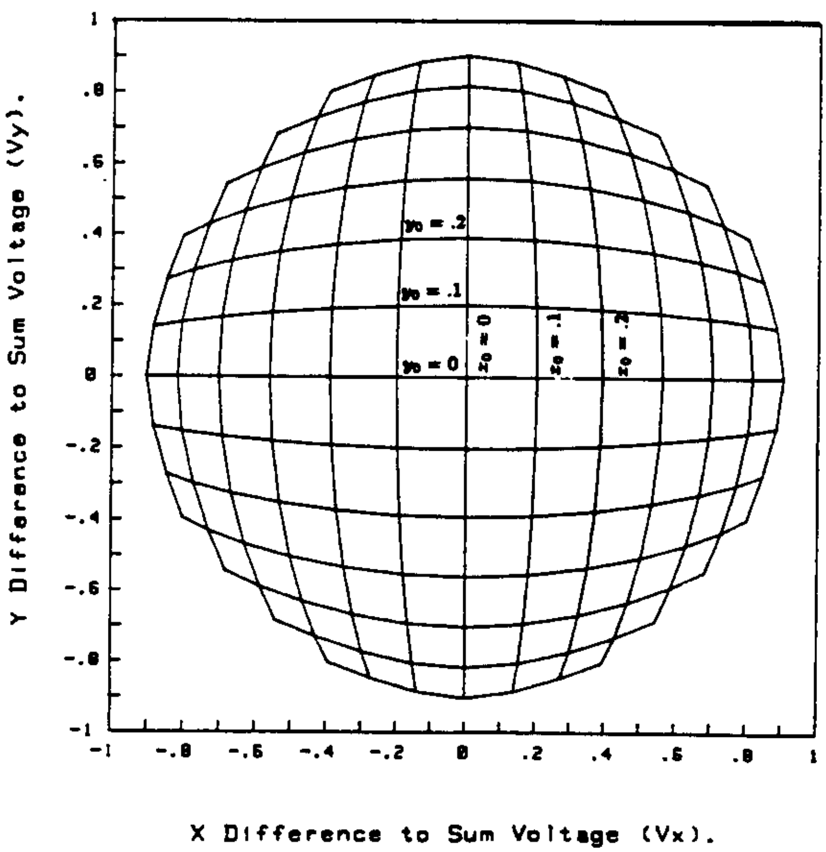

Figure 5. Planar loop monitor.
Lines of constant x_0 and y_0 in difference to sum voltage plane.

In (13), ϕ_s is the initial angle of the helix at $z = 0$ (shown as 0° for the loop
3b). Using (13) in (10) and (11) results in an expression similar to (12) for th
inductance between the beam and the helical pickup:

$$M(r_0, \phi_0, \phi_s) = \frac{\mu_0 l}{4\pi^2} \int_0^{\pi} \ln\left[\frac{b^2 r_0^2 - 2br_0 \cos(\theta + \phi_s - \phi_0) + 1}{r_0^2 - 2br_0 \cos(\theta + \phi_s - \phi_0) + b^2}\right] d\theta \ .$$

The values of ϕ_s for the four pickups of a complete monitor are given as:

M	ϕ_s
M_x^+	$3\pi/2$
M_x^-	$\pi/2$
M_y^+	0
M_y^-	π

Table 2. Helical loop pickup angles.

Plots similar to those of Figures (4) and (5) for the helical pickups are shown in Fi
(6) and (7). In constructing the plots, the integral in (14) was evaluated numericall
b was again assumed to be .7. From Figure 6, it is evident that a certain degr
linearity has been achieved for values of ϕ_0 up to 45°. However, Figure 7 reveals th
and V_y are still strongly dependent on both position variables outside the region r_0
In addition, the smaller grid sections in the mapping for the helical loops indicates
position sensitivity. This point will be examined in more detail in the next section
view of its limited advantages over the planar loop monitor and mechanical comple
the helical monitor was deemed to be impractical.

Pickup Impedances for Loop Monitors

In this section, two useful figures of merit, the longitudinal and transverse pic
impedances, are calculated for the loop monitor. The longitudinal pickup impedanc
defined as the sum voltage from a pickup pair divided by the beam current for a cente
beam. For symmetrical monitors, the x and y longitudinal impedances are identical
are designated by $Z_{\|}$. Using the x axis pickups, $Z_{\|}$ may be written:

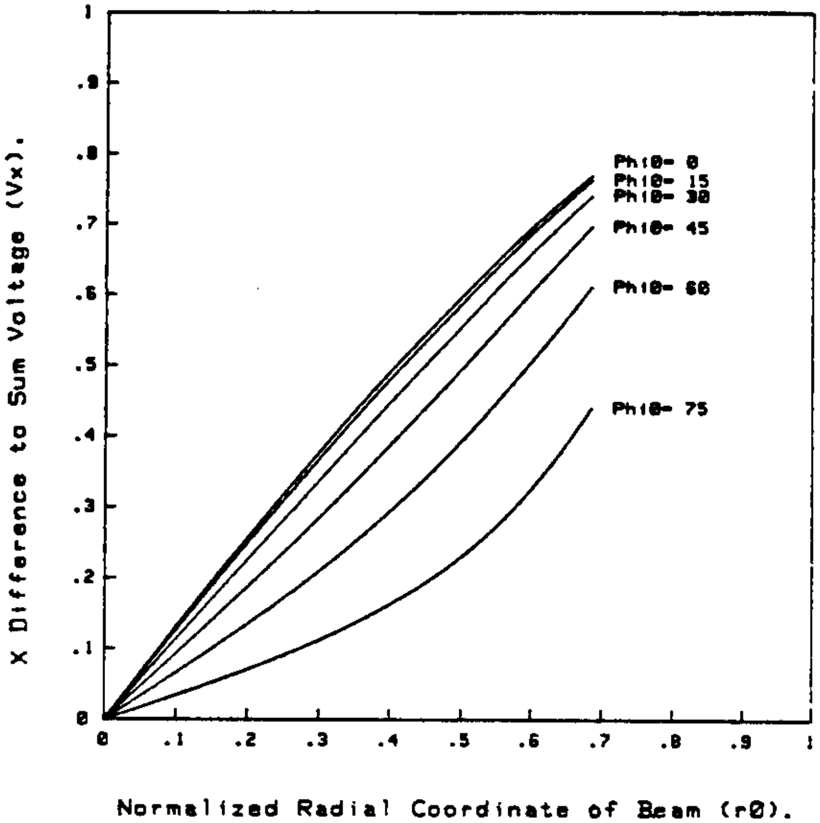

Figure 6. Helical loop monitor. V_x verses r_0 for several values of ϕ_0.

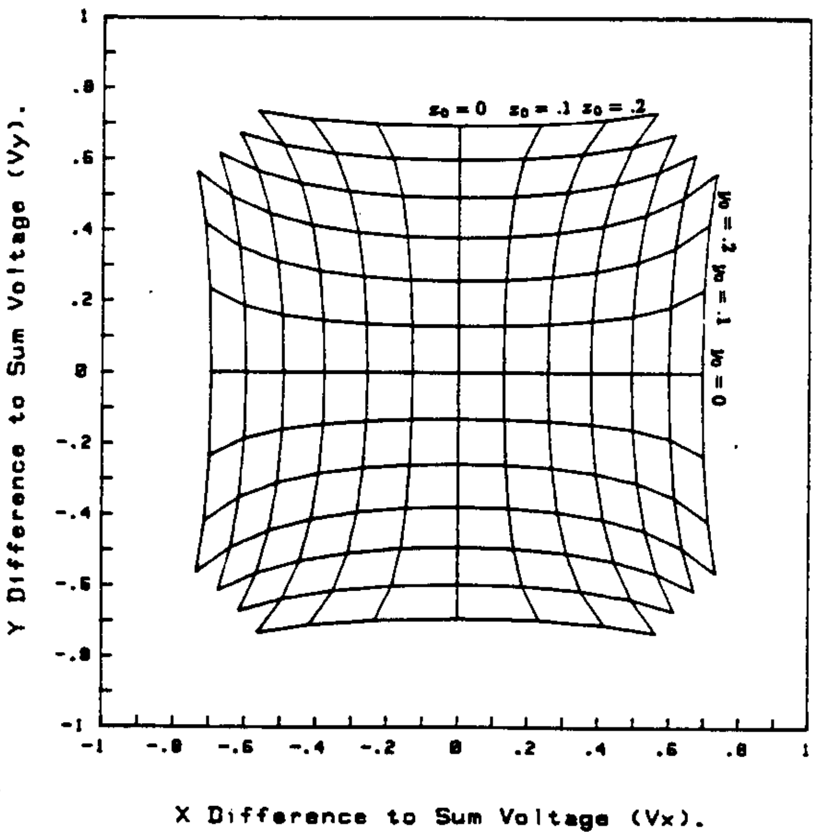

Figure 7. Helical loop monitor.
Lines of constant x_0 and y_0 in difference to sum voltage plane.

$$Z_{\parallel} = \frac{1}{I_b} V_{\Sigma x}\Big|_{r_0=0} = jw(M_x^+ + M_x^-)\Big|_{r_0=0} . \tag{15}$$

Using equation (12) with $r_0 = 0$, the expression for $Z_{\parallel}$ becomes:

$$Z_{\parallel} = \frac{jw\mu_0 l}{\pi} \ln \frac{1}{b} \quad [\Omega] . \tag{16}$$

The transverse pickup impedance relates the change in difference voltage for a pickup pair to a change in beam position along the axis connecting the pickup pair. Again, for symmetrical monitors, the x and y transverse impedances are identical and may be defined using the x axis pickups:

$$Z_{\perp}(x_0) = \frac{1}{I_b} \frac{\partial V_{\triangle x}}{\partial x_0}\Big|_{y_0=0} = jw \frac{\partial}{\partial x_0}(M_x^+ - M_x^-)\Big|_{y_0=0} . \tag{17}$$

Unless the difference voltage is linear, $Z_{\perp}$ will be a function of position. However, it is common practice to define $Z_{\perp}$ for small displacements from the origin. Under this condition, $Z_{\perp}$ may be found by substituting (12) into (17) with $\phi_0 = 0$, differentiating with respect to r_0 and taking the limit as $r_0 \to 0$. The resulting expression for $Z_{\perp}$ is:

$$Z_{\perp} = \frac{jw\mu_0 l}{\pi} \frac{(1 - b^2)}{b} \qquad [\Omega]. \tag{18}$$

In (18) the units of $Z_{\perp}$ are ohms per unit distance normalized to the beampipe radius a. $Z_{\perp}$ may also be expressed in terms of $Z_{\parallel}$:

$$Z_{\perp} = \frac{b^2 - 1}{b \ln b} Z_{\parallel} . \tag{19}$$

Additional information regarding the position sensitivity of the loop monitor may be obtained from $Z_{\parallel}$ and $Z_{\perp}$. For small values of x_0, $V_{\Sigma x} = Z_{\parallel} I_b$ and $V_{\triangle x} = Z_{\perp} I_b x_0$. Therefore, the x difference to sum voltage is:

$$V_x = \left(\frac{Z_\perp}{Z_\parallel}\right) x_0 \qquad x_0 << 1 \ . \tag{20}$$

Hence the ratio $Z_\perp/Z_\parallel$ gives the slope of the difference to sum voltage curve for beam positions on the x or y axis near the origin. From (19) the slope is:

$$m = \frac{b^2 - 1}{b \ln b} \ . \tag{21}$$

For b=.7, m is 2.04. This value is easily verified by examining the $\phi_0 = 0$ curve in Figure 4. A Taylor series expansion of (21) about $b = 1$ shows, that for $b \geq .6$, the approximation $m \approx 2$ is accurate to better than 5% and is exact in the limit $b \rightarrow 1$. It is interesting to note that $m \approx 2$ is, in general, characteristic of all coaxial type position monitors (i.e., loop, capacitive plate, stripline), provided the pickup elements do not subtend angles greater than approximately 25°. For pickups that subtend large angles approaching 180°, the value of m is approximately $4/\pi$. This is the case for the helical monitor because a given pickup subtends 180° of the beam. Examination of the $\phi_0 = 0$ curve in Figure 6 shows that its slope is indeed $4/\pi$ for small values of r_0. In addition, the dimensions of the grid sections near the origin in Figures 5 and 7 are directly proportional to m. Comparing the grid sections shows that the planar loop monitor is about 1.6 or $\pi/2$ times more position sensitive than the helical monitor.

The ratio $m = Z_\perp/Z_\parallel$ is seen to be an important quantity for describing the performance of the loop monitor. It is solely a function of the pickup geometry and defines the position sensitivity of the monitor. A large value of m is desireable for good position resolution. This is best accomplished by decreasing b, but is usually difficult to do in practice without limiting the beam aperture. It is also very important to maximize $Z_\parallel$ and $Z_\perp$ in order to raise the level of the absolute difference and sum signals sufficiently above the noise floor. The simplest method for obtaining high $Z_\parallel$ and $Z_\perp$ internal to the monitor is to use long loops loaded with a high permeability material such as ferrite. As discussed in a latter section, the impedances may also be substantially increased by resonating the pickups and using external voltage step up transformers.

At this point it is worthwhile to restate the important formulas of this section in terms of absolute distances:

$$Z_{\parallel} = \frac{jw\mu_0 l}{\pi} \ln \frac{a}{b} \qquad [\Omega] \tag{22}$$

$$Z_{\perp} \approx \frac{2}{a} Z_{\parallel} \qquad [\Omega/m] \tag{23}$$

$$m \approx \frac{2}{a} \qquad [m^{-1}]. \tag{24}$$

Approximate Expressions for V_x and V_y

For the loop monitor to be a useful device, one must be able to determine beam position from V_x and V_y. In general, this task involves solving equations (2) and (12) for r_0 and ϕ_0. However, these equations are sufficiently complicated that it is impractical to solve them directly. Instead, one of several approximations relating beam position to V_x and V_y can be used. The simplest and most obvious approximation is to assume that V_x and V_y are linear functions of x_0 and y_0 respectively with slope m. However, it was shown in a previous section that this approximation is only valid in the region $r_0 < .2$. Another commonly employed technique involves storing a large number of position/voltage data points determined by calibration on a computer. Position coordinates given V_x and V_y are then found by a search algorithm and some type of interpolation. Although this method is quite accurate, the number of data points required makes calibration cumbersome. In addition, search algorithms can use a significant amount of computer time and are not desireable for real time measurements. As an alternative to these methods, the technique described presently for determining position involves simple approximate expressions for V_x and V_y that are accurate well outside the linear region.

In deriving approximate versions of equations (2) and (12), the polar mapping shown in Figure 8 is of considerable use. Here, circles of different radii in the beam position plane have been mapped by (2) and (12) to the V_x, V_y plane for $b = .7$. It is immediately noted that circles in the position plane are mapped into circles in the V_x, V_y plane for values of r_0 out to .4 and beyond. This suggests the following approximate forms for V_x and V_y:

$$V_x(r_0, \phi_0) \approx V_r(r_0) \cos \phi_0 \tag{25a}$$

$$V_y(r_0, \phi_0) \approx V_r(r_0) \sin \phi_0 \ . \tag{25b}$$

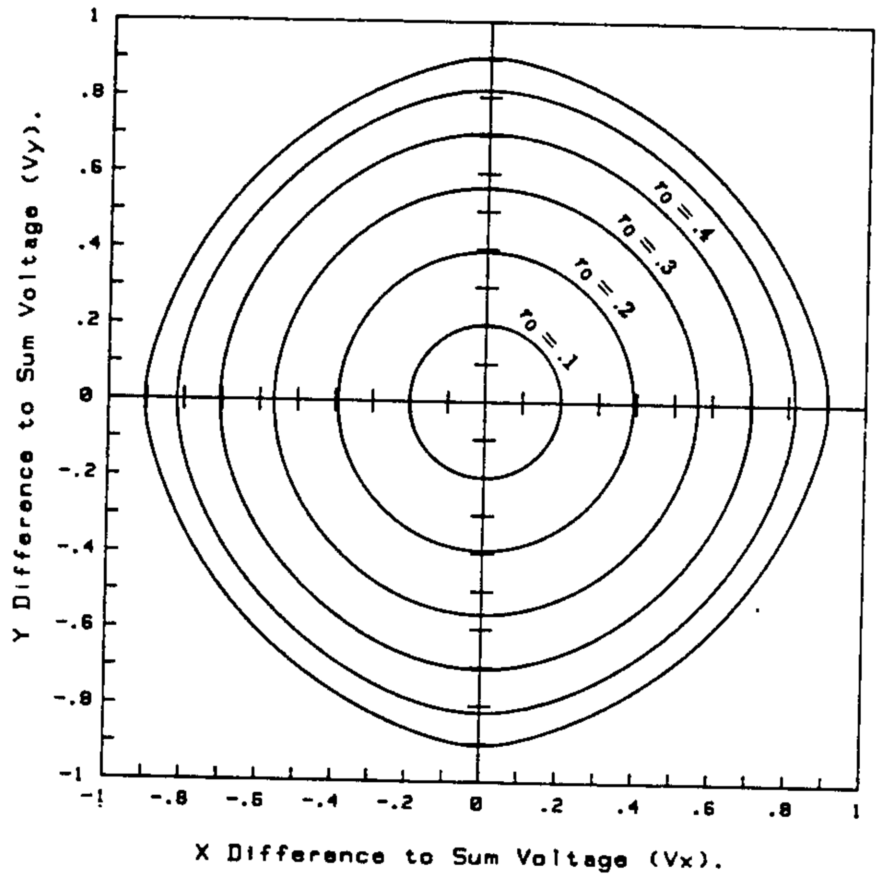

Figure 8 Mapping of circles in position plane to difference to sum voltage plane.

From equations (25), the ϕ_0 coordinate of beam position is found immediately:

$$\phi_0 \approx \tan^{-1}\left(\frac{V_y}{V_x}\right) \quad \text{proper quadrant} \ . \tag{26}$$

It is also evident that:

$$V_r = \sqrt{V_x^2 + V_y^2} \ . \tag{27}$$

From (25a), it is readily seen that $V_r(r_0) = V_x(r_0, 0)$, where V_x is given by equations (2a) and (12). Thus, the $\phi_0 = 0$ curve in Figure 4 is a plot of $V_r(r_0)$. The task now is to find an approximate expression for this curve.

A third order Taylor series expansion of $V_x(r_0, 0)$ about $r_0 = 0$ gives:

$$V_r(r_0) \approx a_0 + a_1 r_0 + a_2 r_0^2 + a_3 r_0^3 \ , \tag{28}$$

where:

$$a_n = \frac{1}{n!} \frac{\partial^n V_x(r_0, 0)}{\partial r_0^n}\bigg|_{r_0=0} \ . \tag{29}$$

In (28), a_0 is obviously zero (see $\phi_0 = 0$ curve in Figure 4). By direct differentiation, a_2 is also found to be zero, and a_1 and a_3 are found to be:

$$a_1 = \frac{b^2 - 1}{b \ln b} \tag{30}$$

$$a_3 = -\frac{1}{6b^3 \ln b}\left[2(1 - b^6) + 3\frac{(1 - b^6)(1 - b^4)}{\ln b}\right] \ . \tag{31}$$

For values of $b > .6$, the approximation $a_1 \approx a_3$ is good to better than 1.25% and is exact in the limit $b \to 1$. For $b = .7$, this approximation is in error by only .3%. It should also be noted that the coefficient a_1 is identically the slope, m, given by (21). Using this information, (28) reduces to:

$$V_r(r_0) \approx m(r_0 - r_0^3) \ . \tag{32}$$

In principle, equation (32) can be solved directly for r_0 in terms of V_r. However, the algebra is complicated and does not yield a compact solution. Instead, another approximation is used. It is noted that the expansion in (32) resembles that of the inverse tangent function. Therefore, let:

$$V_r(r_0) \approx c \tan^{-1} kr_0 \approx ckr_0 - \frac{ck^3 r_0^3}{3} . \tag{33}$$

By equating coefficients of like powers in (32) and (33), the following expressions for c and k are found:

$$c = m/\sqrt{3} \tag{34}$$

$$k = \sqrt{3} . \tag{35}$$

Finally, using (33) and (27), an approximate expression for the radial coordinate is found:

$$r_0 \approx \frac{1}{\sqrt{3}} \tan \frac{1}{m} \sqrt{3(V_x^2 + V_y^2)} . \tag{36}$$

Together, (36) and (26) can be used to determine beam position as a function of x and y difference to sum voltages. In terms of absolute distance, the value of r_0 obtained by (36) should be multiplied by the beampipe radius a.

The accuracy of equations (26) and (36) is illustrated in Figures 9 and 10. Both figures plot, for $b = .7$, the absolute errors in r_0 and ϕ_0 due to the approximations. Here, absolute error is defined as approximate value minus true value. In Figure 9, the error in r_0 and ϕ_0 is plotted as a function of r_0 for several values of ϕ_0. Similarly, in Figure 10 these errors are plotted as a function of ϕ_0 for several values of r_0. From the plots, it is seen that the error in radial position increases with distance from the center of the monitor and is a maximum along the radius at $\phi_0 = 45°$. Referring to Figure 10, for $r_0 = .56$, (80% of the distance to the pickups) the maximum error in r_0 is .072. For the 17.3 mm radius beampipes in the injector and linacs, this translates to a radial position error of 1.25 mm or 13%. For $r_0 = .42$, (60% of the distance to the pickups) the error in radial position is only .43 mm or 6%. For smaller values of r_0 and other angles, the radial error is much less. Figures 9 and 10 also show the error in ϕ_0 is maximum in the $19° - 22.5°$ and $67.5° - 71°$ regions depending on the value of r_0. At 80% of the distance to the pickups the maximum error in ϕ_0 is .65°, at 60% the error is .57°. To summarize, inside the region $r_0 \leq .42$

the approximations (26) and (36) introduce maximum errors in r_0 and ϕ_0 of 6% and .6° respectively. In most cases, the errors are considerably less than these maximums.

In general, the approximation (36), as it stands, is difficult to apply in practice. Because (36) is in terms of normalized slope and distance, a knowledge of the pipe radius, a, is required to apply it to an actual monitor. Although a can be measured physically, the value obtained in this manner will not yield accurate results when used in conjunction with (36) because of differences between the real monitor and the theoretical model. Two of the more obvious faults in the model are the assumption of perfect conductors and infinitesimal loop wires. However, the main assumptions and results leading to (36) are still assumed to be valid for an actual monitor. In particular, in terms of absolute radial coordinate, R_0, V_r is assumed to take the form:

$$V_r(R_0) \approx A_1 R_0 - A_3 R_0^3 \; . \tag{37}$$

From this, a result similar to (36) may be obtained:

$$R_0 \approx \sqrt{\frac{A_1}{3A_3}} \tan \frac{1}{A_1} \sqrt{\frac{3A_3}{A_1}(V_x^2 + V_y^2)} \; . \tag{38}$$

Equations (38) and (26) relate absolute beam position to measured difference to sum voltages. In order to apply (38), the coefficients A_1 and A_3 must first be determined through calibration.

The calibration consists of measuring $V_r = V_x$ for a beam or current on a wire at two known positions on the positive x axis. The two values of R_0 and V_r can then be used in (37) to solve for A_1 and A_3. The resulting coefficients will depend slightly on the choice of calibration positions and will be slightly different from those obtained by a Taylor series expansion. However, it is still reasonable to believe that Figures 9 and 10 provide a good approximate error estimate for this technique. By choosing calibration points close to the origin, the resulting coefficients will resemble those obtained by the Taylor series method. The result of spreading out the calibration points will be to slightly increase accuracy at larger radii and slightly decrease accuracy at small radii.

The approximations and calibration techniques described above assume a symmetric monitor whose physical and electrical centers coincide. The monitors themselves can be constructed to an accuracy of a few mils so that any discrepency between physical and electrical centers should be due to external electronics. By having separate gain adjustments on each of the four pickups, the electrical and physical centers can easily be made to coincide.

Practical Considerations

In this section, some of the practical aspects of a megahertz inductive loop beam position monitor system for CEBAF are discussed. As stated earlier, the virtues of such a system should be low cost and simplicity. When designing the system to meet these goals, the most important considerations are sensitivity and noise. Presently, it is required that the system be able to measure 1 mm displacements of a 1 μA beam.

The behavior of a practical loop monitor is best described using the idealized equivalent circuit model shown in Figure 11. The circuit model is for a single pickup of a complete monitor. In the equivalent circuit, the beam is represented by a current generator. The loop pickup is represented by a mutual inductance, M, and has a self inductance, L. The resistive element takes into account losses in the pickup such as finite loop and beampipe conductivities. In addition, the loops and other parts of the circuit have intrinsic capacitances represented by C. As previously mentioned, a toroidal ferrite core transformer has been added to step up the output voltage. The transformer has the same effect as using an n turn loop pickup, but is conveniently located outside the beampipe. The pickup response is obviously resonant and may be characterized by the overall transfer impedance of the circuit at resonance:

$$Z_T = \frac{V_0}{I_b} = n\omega_0 MQ \ , \tag{39}$$

where:

$$\omega_0 = 1/\sqrt{LC} \tag{40}$$

$$Q = \omega_0 L/R \tag{41}$$

$$M = \frac{\mu_0 l}{2\pi} \ \ln \ \frac{1}{b} \quad \text{for a centered beam} \ . \tag{42}$$

It is clear by comparison with (15) and (17) that, by operating on resonance and using an external transformer, $Z_{\|}$ and $Z_{\perp}$ are increased by the desireable factor nQ.

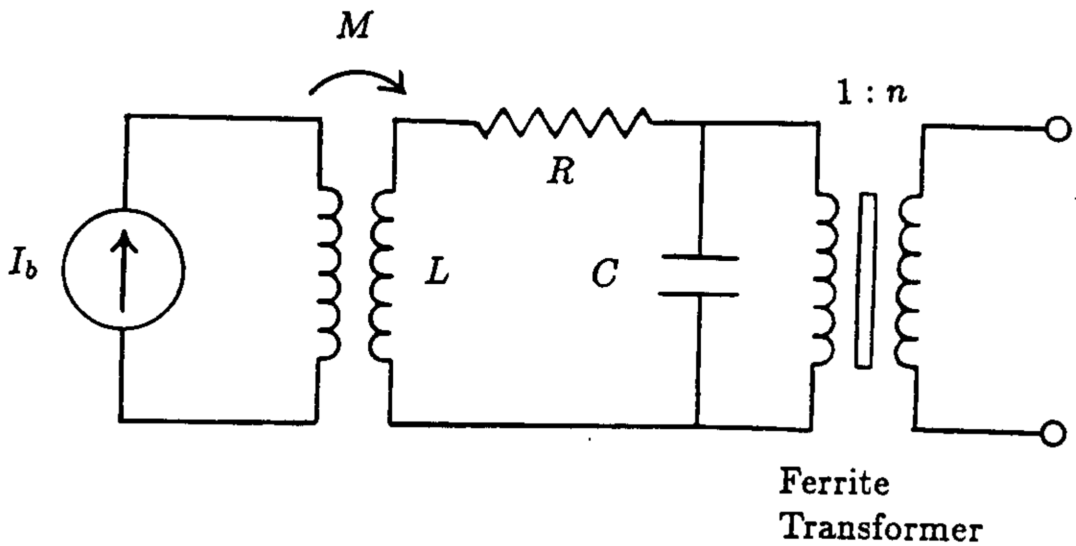

Figure 11 Equivalent circuit of a loop pickup with ferrite core step–up transformer.

It should be stressed that, although the equivalent circuit of Figure 11 is conceptually useful, it is only an idealization and cannot be relied upon to predict pickup impedances. In particular, properties of transformers in the megahertz range may not be ideal. Imperfect, lossy windings give rise to external inductances, capacitances and resistances which alter the resonant frequency and Q of the entire pickup circuit. In addition, the frequency dependence of the core μ' and μ'' further complicates the overall Q and ω_0 of the circuit. Furthermore, the effective turns ratio is usually less than the actual turns ratio because of these effects. Rather than trying to predict these effects with a complicated equivalent transformer circuit, an optimum transformer/loop pickup combination is better determined by trial and error measurements in the laboratory. The measurements are performed using the standard technique of simulating the beam with a thin current carrying wire down the center of the monitor.

For experimental purposes, a single pickup prototype monitor was constructed using standard 1 3/4 " I.D. stainless steel tubing and a copper wire loop. The loop length, l, was

25 cm and the normalized radial distance to the loop was $b = .7$. By experimenting with primary and secondary turns on several different ferrite cores, an optimum transformer was developed for use with the prototype. In general, all of the transformer/pickup combinations yielded resonant frequencies in the 1–10 MHz range. This result along with the availability of simple, low cost electronics in this frequency range, dictates the operating frequency of the monitor system.

For the 25 cm prototype, the optimum transformer consisted of 2 primary turns and 34 secondary turns on a .54 " I.D., .87 " O.D., .25 " wide Krystinel K21 ferrite toroid. The transformer/pickup combination had a resonant frequency of 5 MHz, an overall Q of 30 and an 80Ω transfer impedance. Calculation of M using equation (42) for the prototype yields a value of 1.8×10^{-8} h so that $Z_T = .56\ nQ\ \Omega$. Using the measured value for Z_T implies a value for nQ of 143. Therefore, by adding the ferrite transformer and operating at resonance, the pickup impedances of the monitor were increased by a factor of 143. The total longitudinal and transverse pickup impedances for the prototype/transformer combination are:

$$Z_{||} = 160\ \Omega$$

$$Z_{\perp} \approx 18\ \Omega/\mathrm{mm}\ .$$

Another important component in the loop monitor system is the first stage amplifier at the output of the transformer. The critical characteristic of this amplifier is high impedance so as not to lower the circuit Q. In addition, low noise, high gain, and low input capacitance are also desireable features. For simplicity, OP–37 operational amplifiers in a differential input configuration were used for first stage amplification. With these amplifiers and the prototype monitor, a 1 μA current could be detected. This first result indicates that the inductive loop monitor system is a viable approach for CEBAF. With the incoporation of several improvements to the pickups and electronics, the final monitors are expected to be sensitive enough to cleanly detect displacements of a 100 nA beam.

Lastly, it is pointed out that the preceding measurements and calculations are for the sinusoidal steady state. In reality, repetative bursts of modulation with maximum durations of $\tau = 3.3\ \mu s$ will be detected. Therefore, because of the resonant rise time, the transient pickup impedances will be lower than the steady state values by a factor of:

$$\gamma = 1 - e^{-\omega_0/2Q\ \tau} . \tag{43}$$

For the prototype monitor, the value of γ is .9 for a 4 μs burst and is not considered to be a serious problem. In addition to rise time, the pickups also have a finite fall time. Because of this, the final monitor electronics will include a provision for de–Q–ing the pickups in between bursts.

Current and Future Efforts

As pointed out in the previous section, initial results indicate that the MHz inductive loop monitors show great promise for use at CEBAF. It is clear, however, that much work on the pickups and associated electronics still needs to be completed. Many of the tradeoffs involving ω_0, Q, γ, n and available first stage amplifier gains need to be investigated more thoroughly.

The current concept for the final pickups is illustrated in Figure 12. Here, each loop is separately loaded with a high μ ferrite to increase the transfer impedance, while maintaining position sensitivity. The loops themselves are made of copper and are vacuum deposited directly on the ferrite blocks. As shown in Figure 12, the copper loops completely encircle the ferrite blocks. By cutting the stainless steel beampipe out of the loop circuit, it is hoped that sensitivity will be increased because of reduced losses. In addition, the copper deposited blocks are convenient, self–contained units that are easy to mount and align inside the beampipe.

One concept for the final electronics is presented in Figure 13. The basic system consists of a differential input preamplifier/amplifier and a phase lock loop based heterodyne circuit for low noise signal detection. Several different high frequency, high impedance operational and video amplifiers are currently being evaluated for the preamplifier application. The majority of the phase lock loop detection circuit may be obtained on a single low cost IC chip. To implement the heterodyning technique successfully, some modifications to the basic concept of Figure 13 are expected. In addition, other modulation schemes may also be considered.

At present, a vacuum compatible, wire loop prototype monitor has been constructed and will be installed near the capture section in the injector. This prototype is expected to aid in the evaluation of calibration procedures, external electronics and the feasibility of the modulation concept in general.

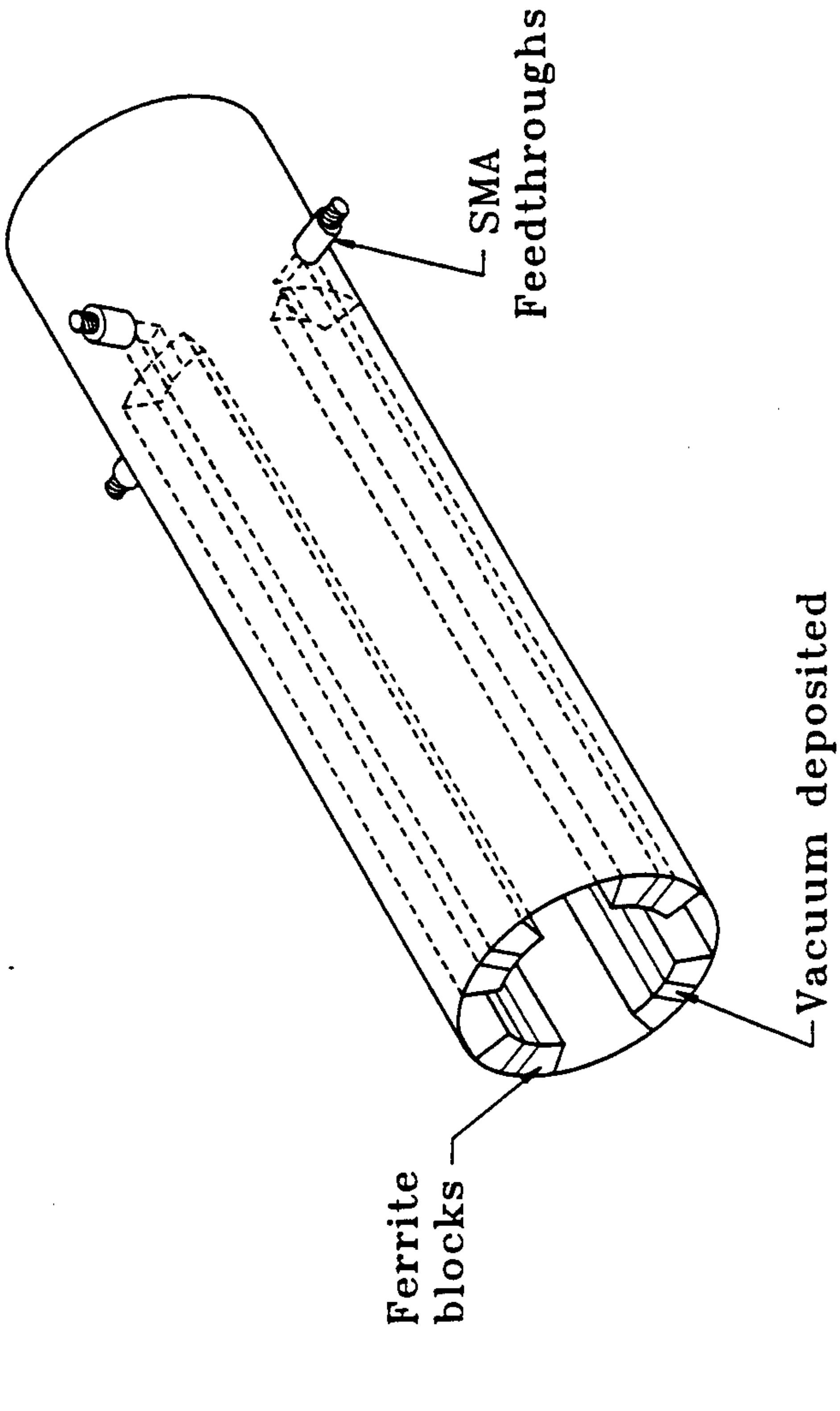

Figure 12 Concept for inductive loop pickups.

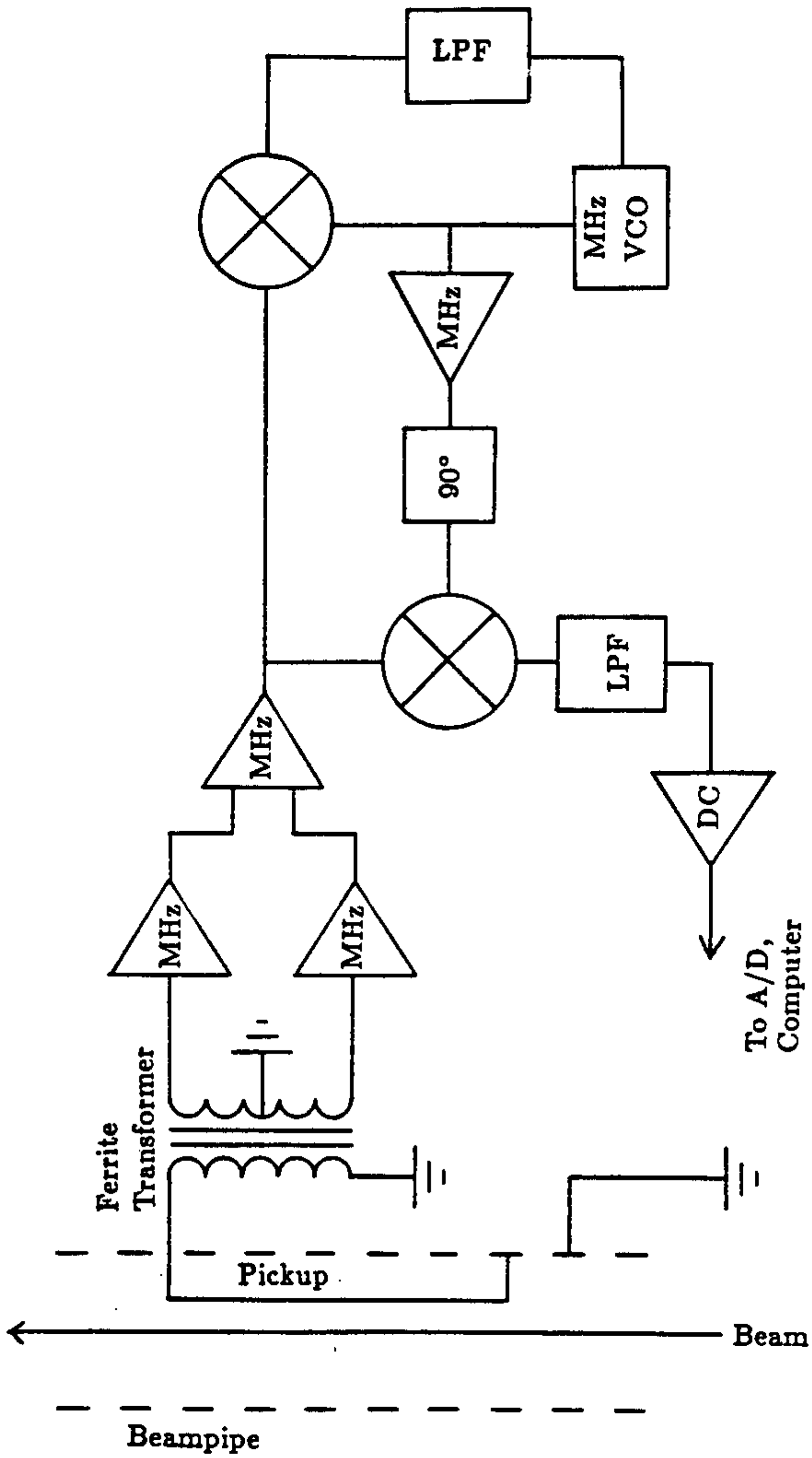

Figure 13 Concept for pickup electronics.

Acknowledgements

The author wishes to express his gratitude to Peter Kloeppel, Geoffrey Krafft and Robert Rossmanith of CEBAF, and Klaus Unser of CERN for many fruitful discussons. In addition, the excellent work of Marty Wise in constructing and evaluating the prototype pickup and electronics was an invaluable contribution. This work was supported by the U.S. Department of Energy under contract DE–AC05–84ER40150.

References

[1] P. Kloeppel, **Beam Diagnostics at CEBAF**, CEBAF–TN–0039, August 1986, pp. 1–6.

[2] S. Ramo, J. Whinnery, and T. Van Duzer, **Fields and Waves in Communication Electronics**, John Wiley and Sons, Inc., New York, 1984, p. 51.